

Limiting Behaviors of Nonconvex-Nonconcave Minimax Optimization via Continuous-Time Systems

Benjamin Grimmer*, Haihao Lu†, Pratik Worah‡, Vahab Mirrokni§

Abstract

Unlike nonconvex optimization, where gradient descent is guaranteed to converge to a local optimizer, algorithms for nonconvex-nonconcave minimax optimization can have topologically different solution paths: sometimes converging to a solution, sometimes never converging and instead following a limit cycle, and sometimes diverging. In this paper, we study the limiting behaviors of three classic minimax algorithms: gradient decent ascent (GDA), alternating gradient decent ascent (AGDA), and the extragradient method (EGM). Numerically, we observe that all of these limiting behaviors can arise in Generative Adversarial Networks (GAN) training. To explain these different behaviors, we study the high-order resolution continuous-time dynamics that correspond to each algorithm, which results in the sufficient (and almost necessary) conditions for the local convergence by each method. Moreover, this ODE perspective allows us to characterize the phase transition between these different limiting behaviors caused by introducing regularization in the problem instance.

1 Introduction

In this paper, we are interested in the limiting behavior of optimizing nonconvex-nonconcave problems

$$\min_{x \in \mathbb{R}^n} \max_{y \in \mathbb{R}^m} L(x, y), \quad (1)$$

for any differentiable loss function $L(x, y)$. Minimax optimization has found wide usage in robust optimization (Verdu and Poor, 1984; Ben-Tal et al., 2009; Bertsimas et al., 2011) and many machine learning tasks. One notable application is in GAN training (Goodfellow et al., 2014) with a generator trying to produce fake data samples G from a latent distribution and a discriminator D trying to distinguish these from true data, defined by the following minimax problem

$$\min_G \max_D \mathbb{E}_{s \sim p_{data}} [\log D(s)] + \mathbb{E}_{e \sim p_{latent}} [\log(1 - D(G(e)))]. \quad (2)$$

*bdg79@cornell.edu; Cornell University, Ithaca NY

†Haihao.Lu@chicagobooth.edu; Google Research, New York NY and University of Chicago, Chicago IL

‡pworah@google.com; Google Research, New York NY

§mirrokni@google.com; Google Research, New York NY

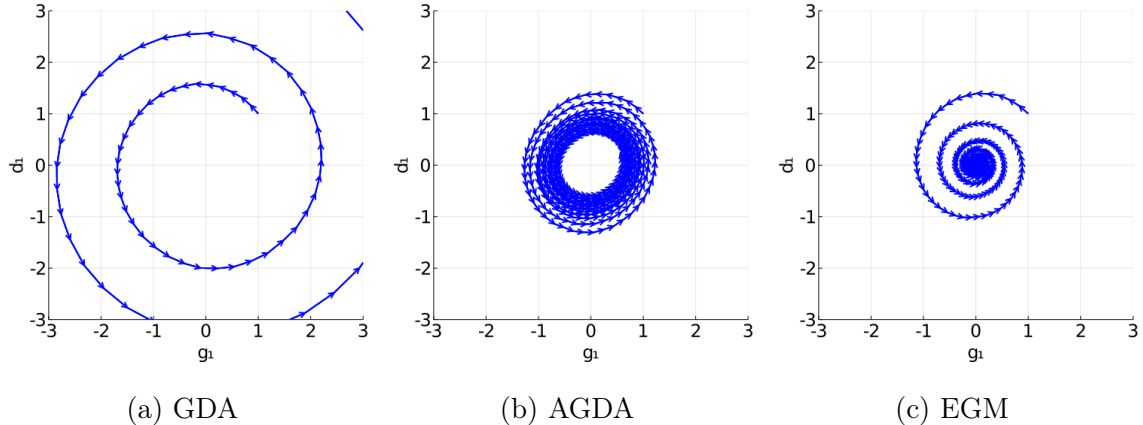


Figure 1: Sample trajectories of GDA, AGDA, and EGM with batch size 1000 applied to a simple GAN (2) showing the first coordinate of g and d which diverge, cycle, and converge around a stationary point at the origin.

We consider first-order methods for solving (1) given a gradient oracle

$$F(x, y) = (\nabla_x L(x, y), -\nabla_y L(x, y))$$

or an unbiased estimator of these gradients. Given such an oracle, three of the most classic first-order minimax optimization methods can be defined as follows, producing a sequence of solution pairs $z_k = (x_k, y_k)$:

Gradient Descent Ascent (GDA)

$$z_{k+1} = z_k - sF(z_k), \tag{3}$$

Alternating Gradient Descent Ascent (AGDA)

$$\begin{aligned} x_{k+1} &= x_k - sF_x(x_k, y_k) \\ y_{k+1} &= y_k - sF_y(x_{k+1}, y_k), \end{aligned} \tag{4}$$

and the Extragradient Method (EGM)

$$\begin{aligned} z_{k+1/2} &= z_k - sF(z_k) \\ z_{k+1} &= z_k - sF(z_{k+1/2}). \end{aligned} \tag{5}$$

Stochastic versions of these algorithms all follow by replacing $F(x, y)$ with an unbiased estimator. In the case of GAN training, an unbiased gradient estimate is given by using a finite batch of samples from p_{data} and p_{latent} to approximate the expectations in (2).

We begin by considering the limiting behavior of these three methods on a GAN training example over CIFAR-10 data (with full experiment details given in Section 2). We take simple models for the discriminator controlling weights $d \in \mathbb{R}^n$ in a logistic

$$D(s) = \frac{1}{1 + e^{d^T(s-\bar{s})}} \tag{6}$$

where $\bar{s} = \mathbb{E}_{s \sim p_{data}}[s]$ is the average image over the dataset and the generator controlling a translation of a normal latent distribution $g \in \mathbb{R}^n$ giving $G(e) = g + e$. Figure 1 shows that even in this simplified setting the trajectories of GDA, AGDA, and EGM vary greatly, diverging, cycling, and converging respectively.

There has been a recent surge in using continuous time ODE models to understand the behavior of iterative optimization methods, initiated by Su et al. (2016). A typical focus is on the ODE arising from taking the stepsize $s \rightarrow 0$ to zero. However, under this limit, all three of these methods have their solution paths converge to the *gradient flow* (GF) given by the ODE

$$\dot{z} = -F(z). \tag{7}$$

To understand the differences in limiting behavior we have observed between GDA, AGDA, and EGM, we need to consider the $O(s)$ -resolution ODEs proposed by Shi et al. (2018) and Lu (2020), which capture differences between these methods when the stepsize s is nonzero.

1.1 Our Contributions

The main contributions of this work is understanding and characterizing different possible (potentially nonconvergent) limiting behaviors and limit points of minimax algorithms, which enables us to explain the differing trajectories observed in our one-layer GAN example.

1. **Divergence, cycling and limit points.** We derive necessary and sufficient conditions for stationary points to be attractive for each of GDA, AGDA, and EG of the generic minimax problem (1). These conditions apply broadly to any sufficiently differentiable nonconvex-nonconcave minimax problems and explain the differences in convergence and divergence found in our GAN experiments. Our conditions are based on understanding the underlying ODEs, but apply directly to each discrete-time algorithms.
2. **Regularization induced phase transitions.** Adding regularization into our our one-layer CIFAR example eventually leads GDA and AGDA to converge. As the regularization parameter increases, Figure 2 shows AGDA has its attractive limit cycle shrink, eventually collapsing into an attractive stationary point. Figure 3 shows a different phase transition occurring where GDA has a stationary point at the origin change from being repulsive to locally attractive with increasing radius of attraction. As regularization is added, a phase transition occurs producing an attractive limit point. For a broad class of problems, this transition will be a Hopf bifurcation. We present polynomial examples demonstrating Hopf bifurcations occurring in minimax optimization and use them to explain the transitions from divergence and cycling to convergence observed in Figures 2 and 3.

1.2 Related Works

Divergence and cycling. GDA is well known to diverge even for convex-concave problems while EGM still converges, the simplest example being $\min_{x \in \mathbb{R}} \max_{y \in \mathbb{R}} xy$. Cycling behaviors arising in nonconvex-nonconcave problems have been observed in a variety of different settings (Letcher, 2020; Hsieh et al., 2020; Grimmer et al., 2020). We differ from these works

in that our focus is on developing tools for characterizing attractive limit points and the transitions between different limiting behaviors for a wide range of minimax algorithms.

GAN equilibriums. Arora et al. (2017) showed under moderate size requirements, GAN training will have an approximately pure equilibrium but that equilibrium point may be far from target true data distribution. These results however do not guarantee that an equilibrium point will be found, leaving the potential for cycling and divergence as seen in Figure 1.

Nonconvex-nonconcave limit points. Quantifying limit points as local Nash equilibrium with measures like stationarity $\nabla L(x, y) \approx 0$ (which is the first-order necessary condition for a Nash equilibrium) has been done for a variety of different first-order methods (Cherukuri et al., 2016; Daskalakis and Panageas, 2018; Adolphs et al., 2019; Mazumdar et al., 2020; Liang and Stokes, 2019). We follow in this vein as the limit points of GDA and AGDA necessarily have $\nabla L(x, y) = 0$.

Alternative measures of local optimality are discussed in Jin et al. (2020), where a notion of local minimax points is presented capturing the sequential nature of minimax problems and relating to GDA’s limit points.

Nonconvex-nonconcave convergence rates. Beyond characterizing the limit points, there has also been a recent push to establish finite-time convergence guarantees for nonconvex-nonconcave minimax problems. Many of these approaches rely on forms of convex-concave-like assumptions, such as Minty’s Variational Inequality (Lin et al., 2018) and Polyak-Lojasiewicz conditions (Nouiehed et al., 2019; Yang et al., 2020). For nonconvex-nonconcave problems of the form $L(x, y) = f(x) + x^T Ay - g(y)$, linear convergence occurs when the interaction between the minimizing and maximizing agents is sufficiently strong or sufficiently weak (Grimmer et al., 2020). The limitation to these convex-concave like assumptions or bilinear structure however prevents these results from describing the phenomena observed herein for GANs.

2 GAN Divergence, Cycling and Phase Transitions

As briefly described in the introduction, we begin by surveying the types of solution paths that arise numerically from GAN training (2). We fix the true data distribution p_{data} as being uniformly over the set of 50,000 training images in the CIFAR-10 dataset, each represented as vectors of length $n = 32 \times 32 \times 3$ and the latent distribution p_{latent} as a standard normal.

We find that considering one-layer networks already suffices to encounter a wide range of different solution path geometries when solving (2). We consider a discriminator controlling weights $d \in \mathbb{R}^n$ in the logistic (6) and a generator controlling a translation $g \in \mathbb{R}^n$ giving $G(e) = g + e$.

For this setup, we find that the origin $(g, d) = (0, 0)$ has $F(0, 0) \approx (0, 0)$ and so it is an approximate stationary point for all three of GDA, AGDA, and EGM. However, the solution paths of these methods vary widely when initialized near the origin at $g = (1, 0, \dots, 0)$ and $d = (1, 0, \dots, 0)$ with fixed $s = 0.2$, not all converging to the origin. Sample solution paths using batches of 1000 samples to approximate the gradients are shown in Figure 1, plotting

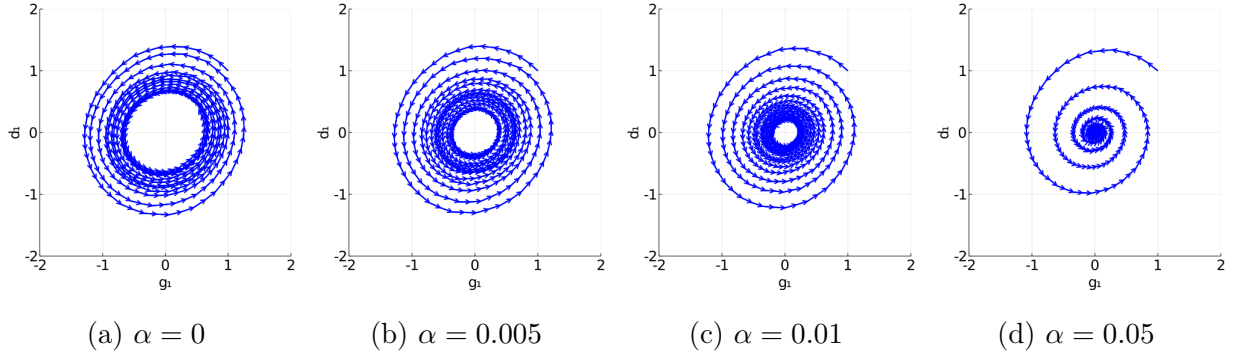


Figure 2: AGDA trajectory on a simple GAN with increasing quadratic regularization.

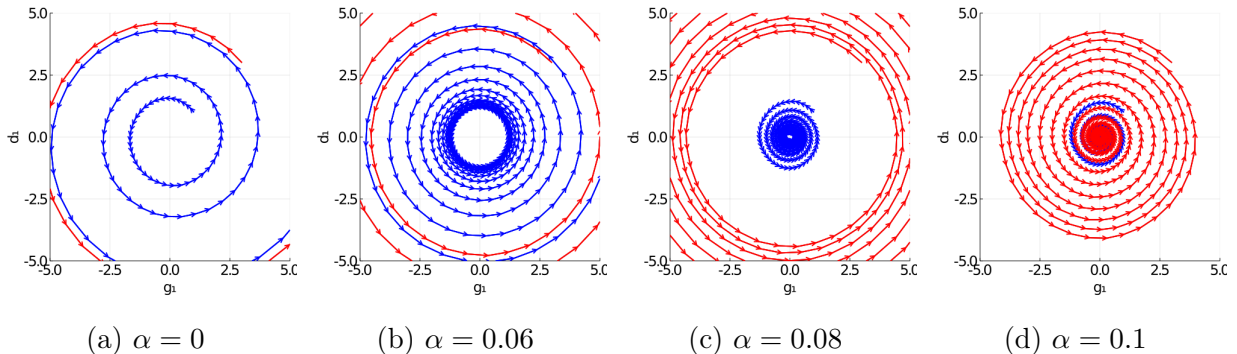


Figure 3: GDA trajectories on a simple GAN from two initializations with increasing quadratic regularization.

the first coordinate of g and d which had the only nonzero initializations. Appendix A gives more sample trajectories using smaller batch sizes, showing the same general dynamics hold but noisier.

This experiment shows three different limiting behaviors arising: GDA diverges spiraling outward from the origin, AGDA falls into a stable cycle around the origin, and EGM converges into a stationary point around the origin. In Section 3, we develop theory based on related $O(s)$ -resolution ODE models explaining these observed differences in convergence and divergence.

Since GDA and AGDA failed to converge, a typical recourse is to add regularization to the objective to deter this behavior. Using L2 penalization, we have the modified training problem objective

$$\mathbb{E}_{s \sim p_{data}} [\log D(s)] + \mathbb{E}_{e \sim p_{latent}} [\log(1 - D(G(e)))] + \frac{\alpha}{2} \|g\|^2 - \frac{\alpha}{2} \|d\|^2,$$

for any level of regularization $\alpha \geq 0$. Adding mild amounts of regularization $\alpha < 0.1$ suffices to cause the nonconvergent trajectories of GDA and AGDA to transition into being convergent paths.

Figure 2 shows the trajectory of AGDA (4) as the regularization parameter increases. We see that as α grows larger, the stable limit cycle shrinks until it collapses to a point for some critical value of α between $\alpha = 0.01$ and 0.05 . For all α larger than this critical point, the trajectory of AGDA has transitioned from nonconvergent cycling to convergence.

Figure 3 shows the trajectories of GDA (3) when initialized at $g = d = (1, 0, \dots, 0)$ and at the farther out point $g = d = (3, 0, \dots, 0)$ as regularization grows. For small enough α , both trajectories diverge. At a critical point around $\alpha = 0.04$, the origin becomes locally attractive and as α further increases, the nearer trajectory from $g = d = (1, 0, \dots, 0)$ begins to converge. By $\alpha = 0.1$, the radius of attraction has grown, becoming attractive from the farther initialization.

In Section 4, we explain these two observed phase transitions from having a repulsive stationary point at the origin to an attractive one as bifurcations occurring in the related $O(s)$ -resolution ODE for each algorithm.

3 The Attractive Limit Points of the Four Dynamics

Our simple GAN experiments show the trajectories of GDA, AGDA, and EGM can be topologically different. Here we explain such differences by studying the $O(s)$ -resolution ODEs for the three algorithms (which are formally defined in Section 3.1) as well as the simple gradient flow dynamics. From these, we arrive at our main theoretical result Theorem 3.4 in Section 3.2, giving necessary and sufficient conditions for a stationary point to be attractive for these dynamics. Further, Section 3.3 shows that for reasonably small s , these conditions guarantee the discrete-time iterations have a linear attractor whenever their associated ODE does.

For any positive definite $P \succ 0$, let $\|z\|_P^2 = z^T P z$. Our theory applies to an arbitrary stationary point z^* where we denote the second order derivatives of the objective by $A = \nabla_{xx}^2 L(z^*)$, $B = \nabla_{x,y}^2 L(z^*)$, $C = -\nabla_{y,y}^2 L(z^*)$.

3.1 $O(s)$ -Resolution ODE Systems for Discrete-time Algorithms

The traditional way to obtain an ODE for a discrete-time algorithm is to let the stepsize s go to 0. While that may be the easiest and the most natural approach, we never use $s = 0$ in practice, and even worse, the solution trajectory of the resulting ODE and the discrete-time algorithm with any positive stepsize can be topologically different. This is exemplified by the trajectories of GDA, AGDA, and EGM seen in Figure 3 which are topologically different, despite sharing the same ODE when letting the stepsize go to 0, namely gradient flow. In order to overcome such limitations, high-order resolution ODEs (Shi et al., 2018; Lu, 2020) have been proposed recently to study the subtle differences between similar algorithms. We here utilize the framework proposed in Lu (2020) to study the $O(s)$ -resolution ODE for these three algorithms, which, as we will show later, is capable to explain the different behaviors of the algorithms.

More formally, we say an ODE

$$\dot{z} = f_0(z) + s f_1(z) \tag{8}$$

the $O(s)$ -resolution ODE of a discrete-time algorithm with iterate update $z^+ = g(z, s)$ if it satisfies that for any z and $z^+ = g(z, s)$,

$$\|z(s) - z^+\| = o(s^{r+1}) . \tag{9}$$

For stochastic gradients, this can be extended by considering the fluid limit as $z^+ = \mathbb{E} g(z, s)$ given by using large enough batches. It turns out such an ODE (8) is unique for a smooth enough discrete-time algorithm (see Theorem 1 in Lu (2020)) and we herein study the $O(s)$ -resolution ODE of GDA, AGDA and EGM:

Proposition 3.1. 1. **GDA:** The $O(s)$ -resolution ODE of GDA is

$$\dot{z} = -F(z) - \frac{s}{2} \nabla F(z) F(z). \quad (10)$$

2. **EGM:** The $O(s)$ -resolution ODE of EGM is

$$\dot{z} = -F(z) + \frac{s}{2} \nabla F(z) F(z). \quad (11)$$

3. **AGDA:** The $O(s)$ -resolution ODE of AGDA is

$$\dot{z} = -F(z) - \frac{s}{2} \begin{bmatrix} A & B^T \\ B & C \end{bmatrix} F(z), \quad (12)$$

Letting the stepsize go to zero, all three of these ODEs reduce to the previously stated gradient flow ODE (7).

3.2 Local Convergence of the $O(s)$ -Resolution ODE

Armed with these more refined ODEs for GDA, AGDA, and EGM, we can formalize our necessary and sufficient conditions for a limit point to be attractive. For a generic ODE

$$\dot{z} = G(z), \quad (13)$$

we need conditions for when a fixed point z^* to the ODE (13) is attractive, which will translate into our required conditions for the convergence of specific algorithms. The traditional stability theory of ODE says that the attractivity of a fixed point relies on the whether the real part of the every eigenvalue of $\nabla G(z^*)$ is negative, but unfortunately it is not transparent to directly evaluate the eigenvalue structure of $\nabla G(z^*)$ for minimax problems. Instead, in order to take advantage of the structure of minimax problems, we here study whether $\|z(t) - z^*\|_P$ goes to 0 for a positive definite norm matrix P . The natural norm P to use differs for different algorithms.

Definition 3.2. We say a fixed point z^* is a linear attractor to an ODE system (13) in the P norm if there exists $\delta, \rho > 0$ such that for any initial solution $z(0) \in B(z^*, \delta)$, it holds that $\|z(t) - z^*\|_P \leq e^{-\rho t} \|z(0) - z^*\|_P$.¹

Then the linear attractors of our ODEs of interest are characterized as follows.

¹In ODE literature, this convergence rate sometimes is called exponential convergence. Here we choose to call it linear in order to be consistent with the optimization literature.

Theorem 3.3. 1. **GF:** Suppose z^* is a stationary point to GF (7). Then z^* is a linear attractor to GF (7) in Euclidean norm (that is, $P = I$) if it holds that

$$A \succ 0, C \prec 0 \quad (14)$$

and not if either inequality is strictly violated.

2. **GDA:** Suppose z^* is a stationary point to the $O(s)$ -resolution ODE to GDA (10). Then z^* is a linear attractor to (10) in Euclidean norm if

$$A + \frac{s}{2}(A^2 - BB^T) \succ 0, C + \frac{s}{2}(C^2 - B^T B) \succ 0 \quad (15)$$

and not if either inequality is strictly violated.

3. **EGM:** Suppose z^* is a stationary point to the $O(s)$ -resolution ODE to EGM (11). Then z^* is a linear attractor to (11) in Euclidean norm if

$$A - \frac{s}{2}(A^2 - BB^T) \succ 0, C - \frac{s}{2}(C^2 - B^T B) \succ 0 \quad (16)$$

and not if either inequality is strictly violated.

4. **AGDA:** Suppose z^* is a stationary point to the $O(s)$ -resolution ODE to AGDA (12).

Then z^* is a linear attractor to (12) in scaled Euclidean norm with $P = \begin{bmatrix} I & \frac{1}{2}sB^T \\ \frac{1}{2}sB & I \end{bmatrix}$ if

$$\begin{bmatrix} A + \frac{s}{2}A^2 + \frac{s^2}{4}(AB^T B + B^T BA) & \frac{s}{2}(AB^T + B^T C) + \frac{s^2}{4}(A^2 B^T + B^T C^2) \\ \frac{s}{2}(B^T A + CB) + \frac{s^2}{4}(BA^2 + C^2 B) & C + \frac{s}{2}C^2 + \frac{s^2}{4}(CBB^T + BB^T C) \end{bmatrix} \succ 0 \quad (17)$$

and not if the inequality is strictly violated.

Similar sufficient conditions for GDA and EGM were presented in Lu (2020). Theorem 3.3 improves upon those by only requiring the positive definiteness conditions to hold only at z^* , whereas Lu (2020) requires similar positive definiteness conditions to hold globally. This difference comes from the analysis utilizing different energy functions.

To prove this theorem, we first establish some basic properties of linear attractors. Consider a fixed point z^* to the generic ODE (13). Suppose the ODE is locally Lipschitz continuous around z^* , i.e., there exists $H > 0$ such that

$$\|\nabla G(z)\| \leq H \text{ for any } z \in \{z \mid \|z - z^*\| \leq 1\}. \quad (18)$$

The following proposition presents a sufficient condition for whether a fixed point is a linear attractor:

Proposition 3.4. Consider a stationary point z^* to the dynamic (13), namely $G(z^*) = 0$. For any positive definite matrix $P \succ 0$, if

$$\frac{1}{2}(\nabla G(z^*)^T P + P \nabla G(z^*)) \prec 0, \quad (19)$$

then z^* is a linear attractor to the dynamic $\dot{z} = G(z)$ in the P norm.

The next proposition shows that the above sufficient condition is essentially tight. The only slack between these results is boundary case when the Jacobian-like term $\frac{1}{2}(\nabla G(z^*)^T P + P \nabla G(z^*))$ is only negative semidefinite, in which case high-order derivatives will determine whether the point is attractive.

Proposition 3.5. *Consider a fixed point z^* to the dynamic (13), namely $G(z^*) = 0$. For any positive definite matrix $P \succ 0$, if*

$$\lambda_{\max} \left(\frac{1}{2} (\nabla G(z^*)^T P + P \nabla G(z^*)) \right) > 0, \quad (20)$$

then z^ is not a linear attractor to the dynamic $\dot{z} = G(z)$ in the P norm.*

Applying these propositions to the four continuous-time dynamics we consider is the core of our proof of Theorem 3.3. One key step in establishing these conditions is choosing the corresponding norms for studying different algorithms. As we can see in Figure 2 and 3, the trajectory of AGDA follows from a slightly skewed ellipsoid while that of GDA is more symmetric. This is fundamentally because GDA has simultaneous updates in primal and dual, while AGDA utilizes sequential updates. This difference results in different choices of norm P when studying the two algorithms. It turns out the natural norms for GF, GDA and EGM are the same: the Euclidean norm with $P = I$, and the natural norm for AGDA is an scaled Euclidean norm with $P = \begin{bmatrix} I & \frac{1}{2}sB^T \\ \frac{1}{2}sB & I \end{bmatrix}$. These norms are obtained by examining the dynamics of each method when solving bilinear systems $L(x, y) = y^T Bx$.

Remark 3.6. *It holds for bilinear problem $L(x, y) = y^T Bx$ that the LHS of (17) is 0. This explains the circling over an ellipsoid behavior of AGDA when solving the bilinear problem. Indeed, the ellipsoid is given by the matrix $P = \begin{bmatrix} I & \frac{1}{2}sB^T \\ \frac{1}{2}sB & I \end{bmatrix}$.*

3.3 Local Convergence of the Discrete-time Algorithms

Here we extend our guarantees from Theorem 3.3 from the underlying ODEs to the discrete-time algorithms. Similar to the results stated in Section 3.2, we first present general results and then apply them to the specific algorithms.

We consider a generic discrete-time algorithm with iterate update $z^+ = g(z, s)$ and the dynamic around a fixed point z^* . As defined in Lu (2020), we say the $O(s)$ -resolution ODE is gradient-based if for any $\delta > 0$, there exists a constant $c > 0$ such that it holds for any $z \in \{\|F(z)\| \leq \delta\}$ and a small enough stepsize s that

$$\|z(s) - z^+\| \leq cs^{r+2}\|F(z)\|, \quad (21)$$

where $z^+ = g(z, s)$, and $z(s)$ is the solution obtained at $t = s$ following its $O(s)$ -resolution ODE with initial solution $z(0) = z$. Indeed, the $O(s)$ -resolution ODE of AGDA, EGM, GDA are gradient-based when $L(x, y)$ is smooth enough.

Proposition 3.7. *Suppose $L(x, y)$ is fifth-order differentiable over x and y and $\nabla^j F(z)$ is bounded for $j = 1, 2, 3, 4$. Then $O(s)$ -resolution ODE of AGDA, EGM, GDA are gradient-based.*

Using this condition, we find that if the z^* is a linear attractor to the $O(s)$ -resolution ODE, then it is also a linear attractor to the discrete-time algorithm.

Theorem 3.8. *Consider a discrete-time algorithm with iterate update $z^+ = g(z, s)$, and its $O(s)$ -resolution ODE (13). Suppose the $O(s)$ -resolution ODE is gradient-based. Suppose z^* is a linear attractor to its $O(s)$ -resolution ODE and*

$$\lambda_{max} \left(\frac{1}{2} (\nabla G(z^*)^T P + P \nabla G(z^*)) \right) \geq bs ,$$

with $b > 0$. Then there exists s^ , such that for any $s \leq s^*$, z^* is a linear attractor to the discrete-time algorithm.*

As a direct consequence of Theorem 3.8, we know that the conditions (15), (16) and (17) are sufficient conditions for z^* being an attractive for each of GDA, AGDA and EGM when the stepsize s is reasonably small (i.e., smaller than a constant). Lastly, we note that when the stepsize s is reasonably small, the stationary points of the $O(s)$ -resolution ODEs we have considered so far are indeed also stationary points of $L(x, y)$, completing our recovery from ODE guarantees back to the discrete-time algorithms themselves.

Proposition 3.9. *When the stepsize $s \leq \frac{1}{\gamma}$, the stationary points to the $O(s)$ -resolution ODE of GDA, EGM and AGDA, namely (10), (11) and (12) are also stationary points to the general minimax problem (1).*

4 Phase Transitions between Limit Points and Limiting Cycles

The GAN problem considered in Section 2 demonstrated that divergence, cycling, and convergence all easily arise from a simple formulation of GAN training. Meanwhile, Figures 2 and 3 showed that adding mild amounts of regularization sufficed to cause the trajectories of the considered methods to all transition to convergence. Here we explain these phase transitions in the discrete algorithmic iterations using their related ODEs. We conclude this section by examining a pair of degree four polynomial loss functions numerically and theoretically where phase transitions occur, shown in Figures 4 and 5, mirroring those observed for GANs in Figures 2 and 3. The related $O(s)$ -resolution ODEs for each method allow us to characterize what is happening in these polynomial examples.

In continuous-time dynamical systems, the transformation from an (attractive or repulsive) limit point into a limit cycle (or vice versa) can occur when the eigenvalues of the Jacobian $\nabla G(z)$ transition from being all negative real part to having some nonnegative real values. When exactly one conjugate pair of eigenvalues crosses to having positive real part, the dynamics of the system are described as a *Hopf Bifurcation*.

Such transitions are controlled by this pair of eigenvectors and hence are fundamentally a two-dimensional phenomena. This notion can be generalized to multi-dimension problems using the Central Manifold Theorem (Kelley, 1967), which essentially state that one can locally decompose the multi-dimension spaces into independently evolving dynamics on

one-dimension and/or two-dimension manifold. Thus, one could reparameterize the dynamics $\dot{z} = G(z)$ to isolate these behaviors, however, the details of such an approach are beyond the scope of this work.

To formalize the phase transition of solution path dynamics as a hyperparameter $\alpha \in \mathbb{R}$ changes, we consider families of minimax problems

$$\min_x \max_y L(x, y, \alpha).$$

Then we are interested in how the dynamics of the solution path vary for each of the algorithms GDA, AGDA, and EGM.

For ease of presentation, we consider a two-dimension system that corresponds to a conjugate pair of eigenvalues crossing from negative to positive real part (potentially coming from reparameterizing to isolate the independently evolving two-dimension manifold). We suppose the stationary point of interest occurs at the origin $z = 0$ and the dynamics $\dot{z} = G(z)$ at the critical α^* are in the form

$$\begin{bmatrix} \dot{x} \\ \dot{y} \end{bmatrix} = \begin{bmatrix} 0 & -w \\ w & 0 \end{bmatrix} \begin{bmatrix} x \\ y \end{bmatrix} + \begin{bmatrix} P(x, y) \\ Q(x, y) \end{bmatrix} \quad (22)$$

where $w \neq 0$ and P, Q both have $P(0, 0) = Q(0, 0) = 0$ and $\nabla P(0, 0) = \nabla Q(0, 0) = 0$. Indeed, most of the dynamic around the stationary point $z = 0$ and critical point α^* can be transformed to (22) except for some degenerated cases (Kuznetsov, 1998). For dynamics of the form (22), the shape of Hopf Bifurcation occurring for some critical α^* is determined by the *First Lyapunov Coefficient*, defined as

$$\begin{aligned} l_1(0) = & \frac{1}{8w} (P_{xxx} + P_{xyy} + Q_{xxy} + Q_{yyy}) \\ & + \frac{1}{8w^2} (P_{xy}(P_{xx} + P_{yy}) - Q_{xy}(Q_{xx} + Q_{yy}) - P_{xx}Q_{xx} + P_{yy}Q_{yy}) \end{aligned} \quad (23)$$

where subscripts denote partial derivatives at $(0, 0)$.

Depending on the sign of this coefficient, two types of bifurcations can arise, supercritical and subcritical. These correspond to an attractive limit point transforming into a repulsive limit point surrounded by an attractive limit cycle and a repulsive limit point transforming into an attractive limit point surrounded by a repulsive limit cycle, respectively. These two transitions describe the shape of phenomena seen in our GAN training experiments in Figures 2 and 3. In the following two sections, we present degree four polynomial minimax problems that indeed undergo these transformations both numerically seen by applying the discrete-time iteration of a first-order method and theoretically verified by computing this Lyapunov coefficient of the method's $O(s)$ -resolution ODE.

4.1 Supercritical Hopf Bifurcation

When $l_1(0) < 0$, a supercritical Hopf Bifurcation takes place. This is the case that, as α varies through α^* , an attractive limit cycle collapses into being an attractive limit point (or in reverse, an attractive limit point splits into being an attractive limit cycle).

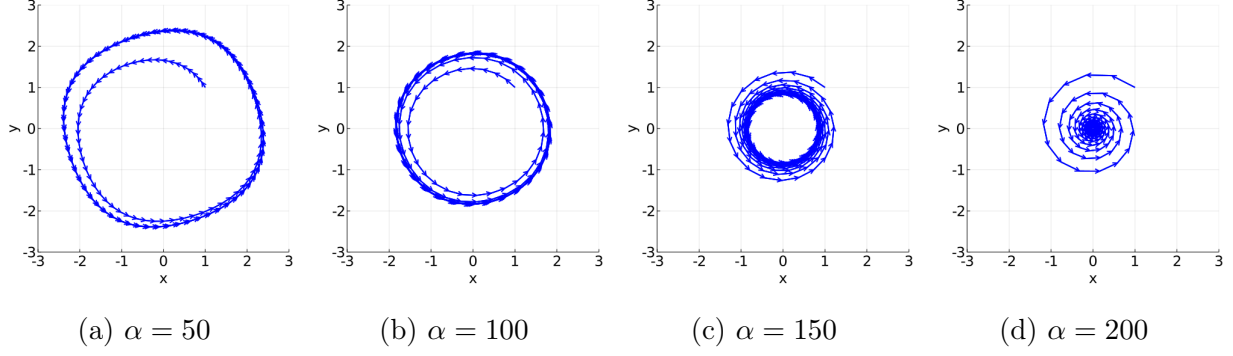


Figure 4: EGM trajectory on (24) undergoing a Supercritical Hopf Bifurcation as α increases.

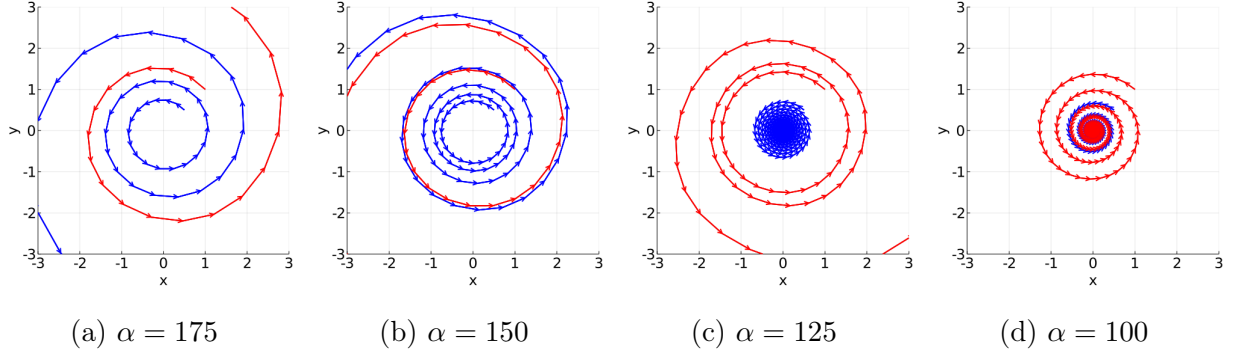


Figure 5: GDA trajectories on (25) undergoing a Subcritical Hopf Bifurcation as α decreases.

Consider the degree four polynomial loss function

$$\min_x \max_y f(x) + \alpha xy - f(y) \quad (24)$$

where $f(x) = (x + 3)(x + 1)(x - 1)(x - 3)$. The behavior of extragradient method with $(x_0, y_0) = (1, 1)$ and $s = 0.002$ as α varies is shown in Figure 4. As α increases past $\alpha^* \approx 165$, the trajectories attractive limit cycle contracts towards the origin, converting the origin from a repulsive limit point to an attractive one.

Considering the related ODE dynamics (11) at $\alpha^* = \sqrt{20400} \approx 143$, the dynamics undergo a supercritical Hopf Bifurcation, which matches the transition we observed in Figure 4. To verify this, we need to verify that these dynamics are of the form (22) and compute the associated first Lyapunov coefficient. This computation is detailed in Appendix C, finding that

$$\begin{aligned} w &\approx 148.542, \\ l_1(0) &\approx -0.04362. \end{aligned}$$

and consequently, this phase transition corresponds to a supercritical bifurcation.

The mild difference between the discrete-time iteration's critical α^* around 165 and the ODE's critical point around 143 is not unexpected as the ODE only approximates the behavior of the first-order method to an accuracy $o(s^2)$. Higher fidelity $O(s^r)$ ODEs could be used following closer to the discrete-time iteration, reducing this difference in when the bifurcation occurs.

4.2 Subcritical Hopf Bifurcation

When $l_1(0) > 0$, a subcritical Hopf Bifurcation occurs. In this case, as α varies through α^* , a repulsive limit cycle collapses into being a repulsive limit point (or in reverse, a repulsive limit point splits into being a repulsive limit cycle, around an attractive limit point).

This behavior can be observed on a degree four polynomial loss function. Consider applying GDA to

$$\min_x \max_y g(x) + \alpha xy - g(y) \quad (25)$$

where $g(x) = -(x+3)(x+1)(x-1)(x-3)$. As α decreases past $\alpha^* \approx 135$, the origin changes from being repulsive to attractive, surrounded by a repulsive cycle. Further decreasing α grows this repulsive cycle, creating a larger area attracted to the origin. Figure 5 shows trajectories initialized at $(1/2, 1/2)$ and $(1, 1)$ which fall into this attractive region by $\alpha = 125$ and $\alpha = 100$, respectively.

Considering the related ODE dynamics (10) at $\alpha^* = \sqrt{20400} \approx 143$, the dynamics undergo a subcritical Hopf Bifurcation, verified in Appendix C as

$$\begin{aligned} w &\approx 148.542, \\ l_1(0) &\approx 0.04362. \end{aligned}$$

Since $l_1(0)$ is positive, this phase transition indeed corresponds to a subcritical bifurcation.

5 Conclusion

Inspired by the topologically different limiting behavior seen by on a one-layer GAN training example, we derived necessary and sufficient conditions for a stationary point to be attractive for each of GDA, AGDA, and EGM that avoid sending the stepsize parameter to zero. These results are based understanding the dynamics of ODEs related to each algorithm, which further allowed us to describe phase transitions in the limiting behavior of these first-order methods, explaining transitions like those we observed when adding regularization to our simplified GAN setting.

References

- Adolphs, L., Daneshmand, H., Lucchi, A., and Hofmann, T. (2019). Local saddle point optimization: A curvature exploitation approach. volume 89 of *Proceedings of Machine Learning Research*, pages 486–495. PMLR.
- Arora, S., Ge, R., Liang, Y., Ma, T., and Zhang, Y. (2017). Generalization and equilibrium in generative adversarial nets (GANs). volume 70 of *Proceedings of Machine Learning Research*, pages 224–232, International Convention Centre, Sydney, Australia. PMLR.
- Ben-Tal, A., El Ghaoui, L., and Nemirovski, A. (2009). *Robust optimization*, volume 28. Princeton University Press.

- Bertsimas, D., Brown, D. B., and Caramanis, C. (2011). Theory and applications of robust optimization. *SIAM review*, 53(3):464–501.
- Cherukuri, A., Gharesifard, B., and Cortes, J. (2016). Saddle-point dynamics: conditions for asymptotic stability of saddle points. arXiv: 1510.02145.
- Daskalakis, C. and Panageas, I. (2018). The limit points of (optimistic) gradient descent in min-max optimization. In *Proceedings of the 32nd International Conference on Neural Information Processing Systems, NIPS’18*, page 9256–9266, Red Hook, NY, USA. Curran Associates Inc.
- Goodfellow, I. J., Pouget-Abadie, J., Mirza, M., Xu, B., Warde-Farley, D., Ozair, S., Courville, A., and Bengio, Y. (2014). Generative adversarial nets. In *Proceedings of the 27th International Conference on Neural Information Processing Systems - Volume 2, NIPS’14*, page 2672–2680, Cambridge, MA, USA. MIT Press.
- Grimmer, B., Lu, H., Worah, P., and Mirrokni, V. (2020). The landscape of nonconvex-nonconcave minimax optimization. arXiv: 2006.08667.
- Hsieh, Y.-P., Mertikopoulos, P., and Cevher, V. (2020). The limits of min-max optimization algorithms: convergence to spurious non-critical sets. arXiv: 2006.09065.
- Jin, C., Netrapalli, P., and Jordan, M. I. (2020). What is local optimality in nonconvex-nonconcave minimax optimization? arXiv: 1902.00618.
- Kelley, A. (1967). The stable, center-stable, center, center-unstable, unstable manifolds. *Journal of Differential Equations*, 3(4):546 – 570.
- Kuznetsov, Y. A. (1998). *Elements of Applied Bifurcation Theory (2nd Ed.)*. Springer-Verlag, Berlin, Heidelberg.
- Letcher, A. (2020). On the impossibility of global convergence in multi-loss optimization. arXiv: 2005.12649.
- Liang, T. and Stokes, J. (2019). Interaction matters: A note on non-asymptotic local convergence of generative adversarial networks. In *The 22nd International Conference on Artificial Intelligence and Statistics*, pages 907–915.
- Lin, Q., Liu, M., Rafique, H., and Yang, T. (2018). Solving weakly-convex-weakly-concave saddle-point problems as successive strongly monotone variational inequalities. arXiv: 1810.10207.
- Lu, H. (2020). An $o(s^r)$ -resolution ode framework for discrete-time optimization algorithms and applications to the linear convergence of minimax problems. arXiv: 2001.08826.
- Mazumdar, E., Ratliff, L. J., and Sastry, S. S. (2020). On gradient-based learning in continuous games. *SIAM Journal on Mathematics of Data Science*, 2(1):103–131.

- Nouiehed, M., Sanjabi, M., Huang, T., Lee, J. D., and Razaviyayn, M. (2019). Solving a class of non-convex min-max games using iterative first order methods. In *Advances in Neural Information Processing Systems 32*, pages 14934–14942. Curran Associates, Inc.
- Shi, B., Du, S. S., Jordan, M. I., and Su, W. J. (2018). Understanding the acceleration phenomenon via high-resolution differential equations. arXiv: 1810.08907.
- Su, W., Boyd, S., and Candès, E. J. (2016). A differential equation for modeling nesterov’s accelerated gradient method: Theory and insights. *Journal of Machine Learning Research*, 17(153):1–43.
- Verdu, S. and Poor, H. (1984). On minimax robustness: A general approach and applications. *IEEE Transactions on Information Theory*, 30(2):328–340.
- Yang, J., Kiyavash, N., and He, N. (2020). Global convergence and variance-reduced optimization for a class of nonconvex-nonconcave minimax problems. arXiv: 2002.09621.

A More trajectories on simple CIFAR GANs

The trajectories presented in Figure 1 all use a large batch size of 1000, which greatly reduces stochastic effects. Figure 5 presents sample trajectories when this batch size is reduced to 1, 10, or 100. Largely, the dynamics of GDA, AGDA, and EGM stay the same. GDA still diverges and AGDA still converges into an attractive limit cycle but with much greater variance in how closely it follows it. EGM still converges towards the origin, eventually staying in a ball around the origin whose radius shrinks as the variance in the gradient samples shrinks.

B Deferred Proofs

B.1 Proof of Proposition 3.1

We utilize Theorem 1 in Lu (2020) and the notations therein to compute the $O(s)$ -resolution ODE.

For GDA and EGM, their $O(s)$ -resolution ODEs are presented in Corollary 1 in Lu (2020). For AGDA, it follows by Taylor expansion of the update rule over stepsize s that

$$z_{k+1} = z_k + sg_1(z_k) + s^2g_2(z_k) + s^3g_3(z_k) + o(s^3) , \quad (26)$$

where $g_1(z_k) = -F(z_k)$, $g_2(z_k) = \begin{bmatrix} 0 \\ \nabla_x F_y(z_k) F_x(z_k) \end{bmatrix}$, and $g_3(z_k) = \begin{bmatrix} 0 \\ -\nabla_{xx} F_y(z_k) (F_x(z_k), F_x(z_k)) \end{bmatrix}$ with $\nabla_{xx} F_y(z_k)$ being a tensor. Now suppose the $O(s)$ -resolution ODE of AGDA is $\dot{z} = f_0(z) + sf_1(z)$, then it follows by Theorem 1 in Lu (2020) that

$$\begin{aligned} f_0(z) &= g_1(z) = -F(z) \\ f_1(z) &= g_2(z) - \frac{1}{2} \nabla f_0(z) f_0(z) = -\frac{1}{2} \begin{bmatrix} A & B^T \\ B & C \end{bmatrix} F(z) . \end{aligned}$$

Hence (12) is the $O(s)$ -resolution ODE of AGDA.

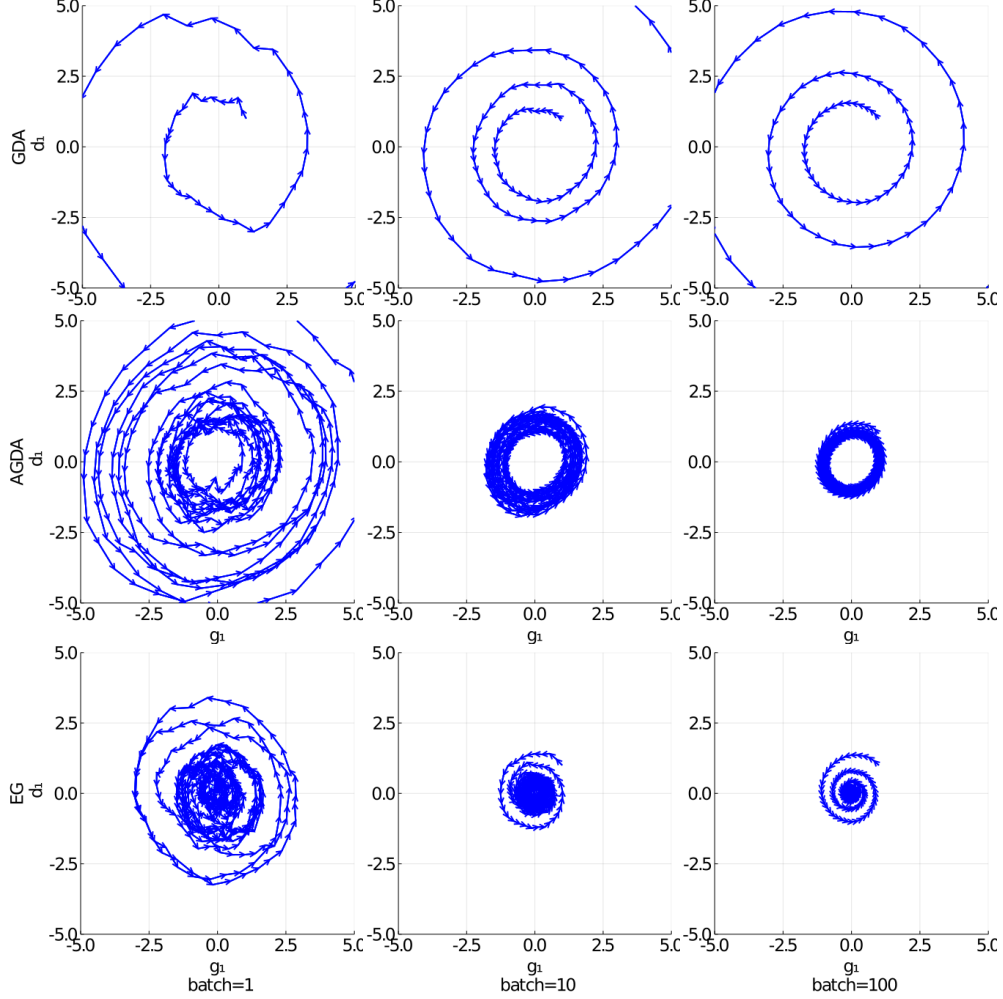


Figure 5: Sample trajectories with smaller batch sizes of 1, 10, and 100 for GDA, AGDA, and EGM on our simplified GAN problem over CIFAR data.

B.2 Proof of Proposition 3.4

We here claim the following fact, which directly proves the proposition: Suppose there exists positive definite matrices $\alpha > 0$ such that

$$\frac{1}{2} (\nabla G(z^*)^T P + P \nabla G(z^*)) \preceq -\alpha I, \quad (27)$$

Let $\bar{P} = \lambda_{\max}(P)$ and $\underline{P} = \lambda_{\min}(P)$ be the maximal and minimal eigenvalue of p.s.d. matrix P . Suppose $H > 0$ satisfies that $\|\nabla^2 G(z)\| \leq H$ for $z \in \{z \mid \|z - z^*\|_P \leq 1\}$ and the initial point $z(0)$ is close enough to z^* : $\|z(0) - z^*\|_P \leq \min\{\frac{\alpha\sqrt{\underline{P}}}{H\bar{P}}, 1\}$, then the trajectory $z(t)$ monotonically converges to z^* with

$$\|z(t) - z^*\|_P^2 \leq e^{-\alpha t/\bar{P}} \|z(0) - z^*\|_P^2. \quad (28)$$

Consider the Lyapunov function $\frac{1}{2}\|z(t) - z^*\|_P^2$. This is monotonically decreasing as

$$\begin{aligned}
\frac{\partial}{\partial t} \frac{1}{2} \|z(t) - z^*\|_P^2 &= (z(t) - z^*)^T P G(z(t)) \\
&\leq (z(t) - z^*)^T P \nabla G(z^*) (z(t) - z^*) + \frac{H\bar{P}}{2} \|z(t) - z^*\|^3 \\
&= \frac{1}{2} (z(t) - z^*)^T (\nabla G(z^*)^T P + P \nabla G(z^*)) (z(t) - z^*) + \frac{H\bar{P}}{2} \|z(t) - z^*\|^3 \\
&\leq -\alpha \|z(t) - z^*\|^2 + \frac{H\bar{P}}{2\sqrt{P}} \|z(t) - z^*\|^2 \|z(t) - z^*\|_P \\
&\leq -\frac{\alpha}{2} \|z(t) - z^*\|^2 \\
&\leq -\frac{\alpha}{2\bar{P}} \|z(t) - z^*\|_P^2,
\end{aligned}$$

where the first inequality utilizes $\|\nabla G(z)\| \leq H$, the second inequality is from (27) and $\|z(t) - z^*\| \leq \frac{1}{\sqrt{P}} \|z(t) - z^*\|_P$, and the third inequality follows from the fact that $\|z(t) - z^*\|_P \leq \frac{\alpha\sqrt{P}}{H\bar{P}}$ by noticing $\|z(t) - z^*\|_P$ is monotonically non-increasing over t . (28) follows immediately from the above inequality.

B.3 Proof of Proposition 3.5

By condition (20), we know that there exists some $\alpha > 0$ such that

$$\lambda_{\max} \left(\frac{1}{2} (\nabla G(z^*)^T P + P \nabla G(z^*)) \right) \geq \alpha I.$$

Let e to be the unit eigenvector of $(\nabla G(z^*)^T P + P \nabla G(z^*))$ that correspond to the max eigenvalue. For any $\delta > 0$, consider taking $z(0) = z^* + \min\{\frac{\alpha}{H\bar{P}}, \delta\}e$. Then it holds that

$$\begin{aligned}
\frac{\partial}{\partial t} \frac{1}{2} \|z(0) - z^*\|_P^2 &= (z(0) - z^*)^T P G(z(0)) \\
&\geq (z(0) - z^*)^T P \nabla G(z^*) (z(0) - z^*) - \frac{H\bar{P}}{2} \|z(0) - z^*\|^3 \\
&= \frac{1}{2} (z(0) - z^*)^T (\nabla G(z^*)^T P + P \nabla G(z^*)) (z(0) - z^*) - \frac{H\bar{P}}{2} \|z(0) - z^*\|^2 \\
&\geq \alpha \|z(0) - z^*\|^2 - \frac{H\bar{P}}{2} \|z(0) - z^*\|^3 \\
&\geq \frac{\alpha}{2} \|z(0) - z^*\|^2 \\
&> 0,
\end{aligned}$$

where the first inequality utilizes $\|\nabla G(z)\| \leq H$, the second inequality is from the definition of $z(0)$, and the third inequality follows from the fact that $\|z(0) - z^*\| \leq \frac{\alpha}{H\bar{P}}$. Therefore, for a smaller enough t , it holds that $\|z(t) - z^*\|_P > \|z(0) - z^*\|_P$, which contradicts with the definition of begin a linear attractor.

B.4 Proof of Theorem 3.3

1. For Gradient Flow (7), we take $P = I$. Notice that

$$\frac{1}{2} (\nabla G(z^*)^T + \nabla G(z^*)) = -\frac{1}{2} (\nabla F(z^*) + (\nabla F(z^*))^T) = \begin{bmatrix} -A & \\ & -C \end{bmatrix} \prec 0,$$

where the inequality is due to (14). Applying Propositions 3.4 and 3.5 with $P = I$ finishes the proof.

2. For Gradient Descent Ascent (10), we take $P = I$. Notice that

$$\begin{aligned} & \frac{1}{2} (\nabla G(z^*)^T + \nabla G(z^*)) \\ &= -\frac{1}{2} (\nabla F(z^*) + (\nabla F(z^*))^T) - \frac{s}{4} ((\nabla F(z^*))^2 + ((\nabla F(z^*))^2)^T) - \frac{s}{4} (\nabla^3 F(z^*)F(z^*) + (\nabla^3 F(z^*)F(z^*))^T) \\ &= -\frac{1}{2} (\nabla F(z^*) + (\nabla F(z^*))^T) - \frac{s}{4} ((\nabla F(z^*))^2 + ((\nabla F(z^*))^2)^T) \\ &= \begin{bmatrix} -A - \frac{s}{2} (A^2 - B^T B) & \\ & -C - \frac{s}{2} (C^2 - B B^T) \end{bmatrix} \\ &\prec 0, \end{aligned}$$

where the second equality is from $F(z^*) = 0$, the third equality uses the definition of $\nabla F(z^*)$ by noticing $\nabla F(z^*)$ and $(\nabla F(z^*))^2$ are both generalized block skew-symmetric, the first inequality utilizes $\|A\|, \| -C \| \leq \|F(z^*)\| \leq 1/s$, and the last inequality is due to (15). Applying Propositions 3.4 and 3.5 with $P = I$ finishes the proof.

3. Similar to 2., we have for EGM (11) that

$$\begin{aligned} & \frac{1}{2} (\nabla G(z^*)^T + \nabla G(z^*)) \\ &= -\frac{1}{2} (\nabla F(z^*) + (\nabla F(z^*))^T) + \frac{s}{4} ((\nabla F(z^*))^2 + ((\nabla F(z^*))^2)^T) + \frac{s}{4} (\nabla^3 F(z^*)F(z^*) + (\nabla^3 F(z^*)F(z^*))^T) \\ &= -\frac{1}{2} (\nabla F(z^*) + (\nabla F(z^*))^T) + \frac{s}{4} ((\nabla F(z^*))^2 + ((\nabla F(z^*))^2)^T) \\ &= \begin{bmatrix} -A + \frac{s}{2} (A^2 - B^T B) & \\ & -C + \frac{s}{2} (C^2 - B B^T) \end{bmatrix} \\ &\prec 0, \end{aligned}$$

where the last inequality is due to (16). Applying Propositions 3.4 and 3.5 with $P = I$ finishes the proof.

4. For Alternating Gradient Descent Ascent (12), we take $P = \begin{bmatrix} I & \frac{1}{2}sB^T \\ \frac{1}{2}sB & I \end{bmatrix}$, and consider $M = \frac{1}{2} (P\nabla G(z^*) + \nabla G(z^*)^T P)$. Then M is symmetric and

$$\begin{aligned} M_{xx} &= -A - \frac{s}{2} A^2 - \frac{s^2}{4} (AB^T B + B^T B A), \\ M_{yy} &= -C - \frac{s}{2} C^2 - \frac{s^2}{4} (C B B^T + B B^T C), \\ M_{xy} &= -\frac{s}{2} (B A + C B) - \frac{s^2}{4} (B A^2 + C^2 B). \end{aligned}$$

Applying Propositions 3.4 and 3.5 finishes the proof.

B.5 Proof of Proposition 3.7

Corollary 2 in Lu (2020) shows that under the condition of Proposition 3.7, the $O(s)$ -resolution ODEs of EGM and GDA are gradient-based. We here just show that the $O(s)$ -resolution ODE of AGDA is gradient-based. Recall the definition of g_1, g_2, g_3 in (26). Notice that under the condition of the proposition, we have $\|g_j(z)\| \leq O(\|F(z)\|)$ and $\|\nabla^k g_j(z)\| \leq O(1)$ for $j = 1, 2, 3$ and $k = 1, \dots, 5 - j$. Thus it follows from Theorem 3 in Lu (2020) that the $O(s)$ -resolution ODE of AGDA is also gradient-based.

B.6 Proof of Theorem 3.8

Suppose $\|z - z^*\| \leq \delta := \min\{\frac{bs\sqrt{\bar{P}}}{H\bar{P}}, 1\}$. Let $z(s)$ be the solution of the $O(s)$ -resolution ODE at $t = s$ from initial solution $z(0) = z$ and $z^+ = g(z, s)$. Then it follows by the proof of Proposition 3.4 that $\|z(s) - z^*\|_P \leq e^{-\frac{1}{2}bs^2/\bar{P}}\|z - z^*\|_P$. Moreover, it follows from the definition of gradient-based $O(s)$ -resolution ODE that there exists $c > 0$ such that $\|z(s) - z^+\| \leq cs^3\|F(z)\|$. Now notice $F(z)$ is Lipschitz continuous in the close and bounded set $B(z^*, \delta)$, i.e., there exists $\gamma > 0$ such that $\|F(z)\| = \|F(z) - F(z^*)\| \leq \gamma\|z - z^*\|$. Putting everything together and letting $s^* = \frac{b\sqrt{\bar{P}}}{8c\gamma\bar{P}^2}$, we have for any $s \leq s^*$ that

$$\begin{aligned}
& \|z^+ - z^*\|_P \\
& \leq \|z(s) - z^*\|_P + \|z^+ - z(s)\|_P \\
& \leq e^{-\frac{1}{2}bs^2/\bar{P}}\|z - z^*\|_P + \bar{P}\|z^+ - z(s)\| \\
& \leq e^{-\frac{1}{2}bs^2/\bar{P}}\|z - z^*\|_P + \bar{P}cs^3\|F(z)\| \\
& \leq \left(1 - \frac{1}{4}bs^2/\bar{P}\right)\|z - z^*\|_P + \bar{P}cs^3\gamma\|z - z^*\| \\
& \leq \left(1 - \frac{1}{4}bs^2/\bar{P}\right)\|z - z^*\|_P + \frac{\bar{P}}{\sqrt{\bar{P}}}cs^3\gamma\|z - z^*\|_P \\
& \leq \left(1 - \frac{1}{8}\frac{bs^2}{\bar{P}}\right)\|z - z^*\|_P,
\end{aligned}$$

where the second inequality utilizes Proposition 3.4 and the definition of \bar{P} , the third inequality utilizes (21), the fourth inequality utilizes $\|F(z)\| = \|F(z) - F(z^*)\| \leq \gamma\|z - z^*\|$ and the last inequality is because $s \leq s^*$. This proves the theorem by telescoping.

B.7 Proof of Proposition 3.9

For GDA, we have $G(z) = -(I + \frac{s}{2}\nabla F(z))F(z)$. Notice $s \leq \frac{1}{\gamma}$, thus it holds that $\|\frac{s}{2}\nabla F(z)\| \leq \frac{1}{2}$, whereby $I + \frac{s}{2}\nabla F(z)$ is a full-rank matrix. Therefore, $G(z) = 0$ is equivalent to $F(z) = 0$, which finishes the proof for GDA. The proof for AGDA and EGM follow the same process.

C Calculation of First Lyapunov Coefficients

We give a proposition providing formulas for $l_1(0)$ for symmetric bilinear problems. Using this formula, we can compute the first Lyapunov coefficient for both polynomial examples considered in Section 4, verifying the phase transitions observed are supercritical and subcritical respectively.

Lemma C.1. *Consider any symmetric and bilinear minimax problem $\min_{x \in \mathbb{R}} \max_{y \in \mathbb{R}} L(x, y, \alpha) = f(x) + \alpha xy - f(y)$ with a stationary point at $(x, y) = (0, 0)$. Then the dynamics of GF (7) at the origin have First Lyapunov Coefficient given by*

$$w = \alpha,$$

$$l_1(0) = -\frac{f^{(4)}(0)}{4\alpha}.$$

The dynamics of GDA (10) at the origin have First Lyapunov Coefficient given by

$$w = \alpha(1 + sf^{(2)}(0)),$$

$$l_1(0) = -\frac{f^{(4)}(0)}{4\alpha(1 + sf^{(2)}(0))} - s\frac{4f^{(4)}(0)f^{(2)}(0) + 3f^{(3)}(0)^2}{8\alpha(1 + sf^{(2)}(0))} + \frac{2sf^{(3)}(0)^2 + 3s^2f^{(3)}(0)^2f^{(2)}(0)}{16\alpha(1 + sf^{(2)}(0))^2}.$$

The dynamics of EG (11) at the origin have First Lyapunov Coefficient given by

$$w = \alpha(1 - sf^{(2)}(0)),$$

$$l_1(0) = -\frac{f^{(4)}(0)}{4\alpha(1 - sf^{(2)}(0))} + s\frac{4f^{(4)}(0)f^{(2)}(0) + 3f^{(3)}(0)^2}{8\alpha(1 - sf^{(2)}(0))} - \frac{2sf^{(3)}(0)^2 - 3s^2f^{(3)}(0)^2f^{(2)}(0)}{16\alpha(1 - sf^{(2)}(0))^2}.$$

Proof. First, we observe that for any problem with $L(x, y, 0) = f(x) + \alpha xy - f(y)$, each of our algorithms give dynamics of the type (22). The symmetry between x and y in the loss function and in EGM and GDA ensures that whenever the trace of $\nabla G(z)$ is zero, the two diagonal entries of $\nabla G(z)$ must be zero.

The dynamics of GF (7) for this class of symmetric problems are given by

$$\begin{bmatrix} \dot{x} \\ \dot{y} \end{bmatrix} = \begin{bmatrix} -f'(x) - \alpha y \\ \alpha x - f'(y) \end{bmatrix}$$

From this, the following derivatives in terms of the form (22) are given by

$$w = Q_x = \alpha,$$

$$P_{xx} = Q_{yy} = -f^{(3)}(0),$$

$$P_{xy} = P_{yy} = Q_{xy} = Q_{xx} = 0,$$

$$P_{xxx} = Q_{yyy} = -f^{(4)}(0),$$

$$P_{xyy} = Q_{xxy} = 0.$$

Then the claimed formula follows from (23).

The dynamics of GDA (10) for this class of symmetric problems are given by

$$\begin{bmatrix} \dot{x} \\ \dot{y} \end{bmatrix} = \begin{bmatrix} -f'(x) - \alpha y \\ \alpha x - f'(y) \end{bmatrix} - \frac{s}{2} \begin{bmatrix} f^{(2)}(x)(f'(x) + \alpha y) - \alpha(\alpha x - f'(y)) \\ \alpha(f'(x) + \alpha y) + f^{(2)}(y)(\alpha x - f'(y)) \end{bmatrix}$$

From this, the following derivatives in terms of the form (22) are given by

$$\begin{aligned} w &= Q_x = a + s\alpha f^{(2)}(0), \\ P_{xx} &= Q_{yy} = -f^{(3)}(0) - \frac{3sf^{(3)}(0)f^{(2)}(0)}{2}, \\ P_{yy} &= -Q_{xx} = \frac{-s\alpha f^{(3)}(0)}{2}, \\ P_{xy} &= Q_{xy} = 0, \\ P_{xxx} &= Q_{yyy} = -f^{(4)}(0) - \frac{s}{2} (4f^{(4)}(0)f^{(2)}(0) + 3f^{(3)}(0)^2), \\ P_{xyy} &= Q_{xxy} = 0. \end{aligned}$$

Then the claimed formula follows from (23).

The dynamics of EGM (11) for this class of symmetric problems are given by

$$\begin{bmatrix} \dot{x} \\ \dot{y} \end{bmatrix} = \begin{bmatrix} -f'(x) - \alpha y \\ \alpha x - f'(y) \end{bmatrix} + \frac{s}{2} \begin{bmatrix} f^{(2)}(x)(f'(x) + \alpha y) - \alpha(\alpha x - f'(y)) \\ \alpha(f'(x) + \alpha y) + f^{(2)}(y)(\alpha x - f'(y)) \end{bmatrix}$$

From this, the following derivatives in terms of the form (22) are given by

$$\begin{aligned} w &= Q_x = a - s\alpha f^{(2)}(0), \\ P_{xx} &= Q_{yy} = -f^{(3)}(0) + \frac{3sf^{(3)}(0)f^{(2)}(0)}{2}, \\ P_{yy} &= -Q_{xx} = \frac{s\alpha f^{(3)}(0)}{2}, \\ P_{xy} &= Q_{xy} = 0, \\ P_{xxx} &= Q_{yyy} = -f^{(4)}(0) + \frac{s}{2} (4f^{(4)}(0)f^{(2)}(0) + 3f^{(3)}(0)^2), \\ P_{xyy} &= Q_{xxy} = 0. \end{aligned}$$

Then the claimed formula follows from (23). □

For the example (24), the function $f(x) = (x + 3)(x + 1)(x - 1)(x - 3)$ has

$$\begin{aligned} f^{(4)}(0) &= 24 \\ f^{(3)}(0) &= 0 \\ f^{(2)}(0) &= -20 \\ f^{(1)}(0) &= 0. \end{aligned}$$

Plugging this into Lemma C.1 yields the EGM ODE dynamics at $\alpha^* = \sqrt{20400}$ having

$$\begin{aligned}
w &= \alpha(1 - sf^{(2)}(0)) = \sqrt{20400}(1 - 0.002 \times -20) \approx 148.542, \\
l_1(0) &= -\frac{f^{(4)}(0)}{4\alpha(1 - sf^{(2)}(0))} + s\frac{4f^{(4)}(0)f^{(2)}(0) + 3f^{(3)}(0)^2}{8\alpha(1 - sf^{(2)}(0))} - \frac{2sf^{(3)}(0)^2 - 3s^2f^{(3)}(0)^2f^{(2)}(0)}{16\alpha(1 - sf^{(2)}(0))^2} \\
&\approx -0.04362.
\end{aligned}$$

Likewise, for (25), the function $g(x) = -(x+3)(x+1)(x-1)(x-3)$ has

$$\begin{aligned}
f^{(4)}(0) &= -24 \\
f^{(3)}(0) &= 0 \\
f^{(2)}(0) &= 20 \\
f^{(1)}(0) &= 0.
\end{aligned}$$

Plugging this into Lemma C.1 yields the GDA ODE dynamics at $\alpha^* = \sqrt{20400}$ having

$$\begin{aligned}
w &= \alpha(1 + sf^{(2)}(0)) = \sqrt{20400}(1 + 0.002 \times 20) \approx 148.542, \\
l_1(0) &= -\frac{f^{(4)}(0)}{4\alpha(1 + sf^{(2)}(0))} - s\frac{4f^{(4)}(0)f^{(2)}(0) + 3f^{(3)}(0)^2}{8\alpha(1 + sf^{(2)}(0))} + \frac{2sf^{(3)}(0)^2 + 3s^2f^{(3)}(0)^2f^{(2)}(0)}{16\alpha(1 + sf^{(2)}(0))^2} \\
&\approx 0.04362.
\end{aligned}$$